NASA TECHNICAL MEMORANDUM

NASA TM X-3137

NASA TM X-3137

EVALUATION OF IMAGE QUALITY IN A CASSEGRAIN-TYPE TELESCOPE WITH AN OSCILLATING SECONDARY MIRROR

E. F. Erickson and S. Matthews

Ames Research Center

Moffett Field, Calif. 94035

NATIONAL AERONAUTICS AND SPACE ADMINISTRATION • WASHINGTON, D. C. • FEBRUARY 1975

1. Report No.	2. Government Accession No.	3. Recipient's Catalog No.
NASA TM X-3137		

4. Title and Subtitle	5. Report Date
EVALUATION OF IMAGE QUALITY IN A CASSEGRAIN-TYPE TELESCOPE WITH AN OSCILLATING SECONDARY MIRROR	February 1975
	6. Performing Organization Code

7. Author(s)	8. Performing Organization Report No.
E. F. Erickson and S. Matthews	A-5657
	10. Work Unit No.
	352-03

9. Performing Organization Name and Address	11. Contract or Grant No.
Ames Research Center, NASA Moffett Field, Calif., 94035	
	13. Type of Report and Period Covered
	Technical Memorandum

12. Sponsoring Agency Name and Address	14. Sponsoring Agency Code
National Aeronautics and Space Administration Washington, D. C., 20546	

15. Supplementary Notes

16. Abstract

This report describes a ray-trace analysis of aberrations and extreme rays of a Cassegrain-type telescope with a tilted secondary mirror. The work was motivated by the need to understand the factors limiting image quality and to assist in the design of secondary mirrors for three telescopes with oscillating secondary mirrors (OSM) used at Ames Research Center for high-altitude infrared astronomy. The telescopes are a 31-cm-diameter Dall-Kirkham (elliptical primary, spherical secondary) flown aboard a Lear jet, a 71-cm balloon-borne Dall-Kirkham flown on the "AIROscope" gondola, and a 91-cm true Cassegrain (parabolic primary, hyperbolic secondary) flown aboard a C-141 jet transport. The optics for these telescopes were not designed specifically for OSM operation, but all have OSM's and all must be used with various detector configurations; therefore, a facility that evaluates the performance of a telescope for a given configuration is useful. The analytical expressions are summarized and results for the above systems are discussed. Details of the calculation and a discussion of the computer program are given in the appendices.

17. Key Words (Suggested by Author(s))	18. Distribution Statement
Telescopes Infrared astronomy Optics	Unclassified - Unlimited STAR Category 35

19. Security Classif. (of this report)	20. Security Classif. (of this page)	21. No. of Pages	22. Price*
Unclassified	Unclassified	25	$3.25

*For sale by the National Technical Information Service, Springfield, Virginia 22151

EVALUATION OF IMAGE QUALITY IN A CASSEGRAIN-TYPE TELESCOPE WITH AN OSCILLATING SECONDARY MIRROR

E. F. Erickson and S. Matthews*

Ames Research Center

SUMMARY

This report describes a ray-trace analysis of aberrations and extreme rays of a Cassegrain-type telescope with a tilted secondary mirror. The work was motivated by the need to understand the factors limiting image quality and to assist in the design of secondary mirrors for three telescopes with oscillating secondary mirrors (OSM) used at Ames Research Center for high-altitude infrared astronomy. The telescopes are a 31-cm-diameter Dall-Kirkham (elliptical primary, spherical secondary) flown aboard a Lear jet, a 71-cm balloon-borne Dall-Kirkham flown on the "AIROscope" gondola, and a 91-cm true Cassegrain (parabolic primary, hyperbolic secondary) flown aboard a C-141 jet transport. The optics for these telescopes were not designed specifically for OSM operation, but all have OSM's and all must be used with various detector configurations; therefore, a facility that evaluates the performance of a telescope for a given configuration is useful. The analytical expressions are summarized and results for the above systems are discussed. Details of the calculation and a discussion of the computer program are given in the appendices.

INTRODUCTION

The requirement of subtracting sky-emission noise in infrared astronomical observations has led to the development of the oscillating secondary mirror (OSM) technique (ref. 1); the secondary mirror in a Cassegrain configuration telescope is positioned alternately at one of two positions so that the detector alternately views two adjacent areas of the sky. The resulting "chopped" detector output is typically processed by a synchronous amplifier (ref. 2) referenced to the OSM motion, thereby providing a dc signal proportional to the difference in the power received from the two areas of the sky. The method has been successful in both airborne and ground-based observations. The principal advantages of the technique are (1) the amount of stray radiation chopped is small and (2) all infrared detection systems to be mounted on the telescope are simplified because the chopper is an integral part of the telescope.

---

*Present address: Physics Dept., Stanford University, Stanford, Calif., 94305.

However, some questions arise concerning the quality of the image in OSM telescopes. For at least one position of the OSM, the axes of the primary and secondary mirrors do not coincide. At wavelengths where thermal emission from the telescope is significant ($1000\mu \geq \lambda \geq 3\mu$), it is desirable to balance the power received by the detector for each of the two mirror positions; therefore, the secondary mirror is typically aligned so that, for the two positions, its axis makes equal and opposite angles with the primary axis. The resulting aberrations can restrict the useful field of view of the instrument. Although diffraction at infrared wavelengths tends to reduce imaging requirements, good spatial resolution of many infrared sources is needed to improve our understanding of them; thus, even in the infrared it is desirable to understand aberrations of the optics. For example, these aberrations determine the wavelength longward of which diffraction effects become dominant. In addition, the quality of the image is an important consideration for multiple-element detector arrays used in conjunction with an OSM telescope.

Also, the possibility of offset guiding by tilting the secondary mirror is limited by the resulting aberrations of the image. This application is the subject of a calculation by Bottema and Woodruff (ref. 3), who summarize third-order aberration constants for well-known Cassegrain-type telescopes and derive the requirements for a configuration with a tilted secondary mirror in which the on-axis image of an off-axis object point is free from third-order coma.

Another unusual requirement for an infrared telescope is that the primary mirror should be "underfilled," that is, the secondary mirror should be undersized to minimize the amount of radiation from the telescope tube seen by the detector. This results in a reduced aperture for which the maximum useful value depends on the tilt of the secondary mirror.

The present report describes a ray-trace analysis of aberrations and extreme rays of a Cassegrain-type telescope with a tilted secondary mirror. This work was motivated by the need to understand limiting image quality and to assist in the design of secondary mirrors for three OSM telescopes used at Ames Research Center for high-altitude infrared astronomy. The telescopes are a 31-cm-diameter Dall-Kirkham (elliptical primary, spherical secondary) flown aboard a Lear jet, a 71-cm balloon-borne Dall-Kirkham flown on the "AIROscope" gondola, and a 91-cm true Cassegrain (parabolic primary, hyperbolic secondary) flown aboard a C-141 jet transport. The optics for these telescopes were not designed specifically for OSM operation, but all have OSM's and all must be used with various detector configurations; therefore, a facility that evaluates the performance of a telescope for a given configuration is useful. Results appropriate to these systems are discussed. Details of the calculation and discussion of the computer program are given in the appendices.

The authors gratefully acknowledge the assistance of Mrs. Mai Liu, who programmed the plot routine for the line printer, Mr. Gordon Augason for useful discussions, and Dr. R. T. Jones for the loan of his notes on Cassegrain-type telescopes.

DESCRIPTION OF CALCULATION

The calculation which follows obtains the intersection with the image-plane of a ray which is incident on the primary at a known radial distance and inclination from the primary axis. The secondary surface is assumed to have its axis tilted from the primary axis by a known angle θ. The image quality is then judged from the distribution of points in the focal plane resulting from a uniform distribution of rays having the same inclination to the primary axis and filling the primary aperture.

The geometry and notation are given in figure 1. Ray L_1 from the object strikes the primary at point A, ray L_2 strikes the secondary at point B, and ray L_3 intersects the image plane at point D. The secondary

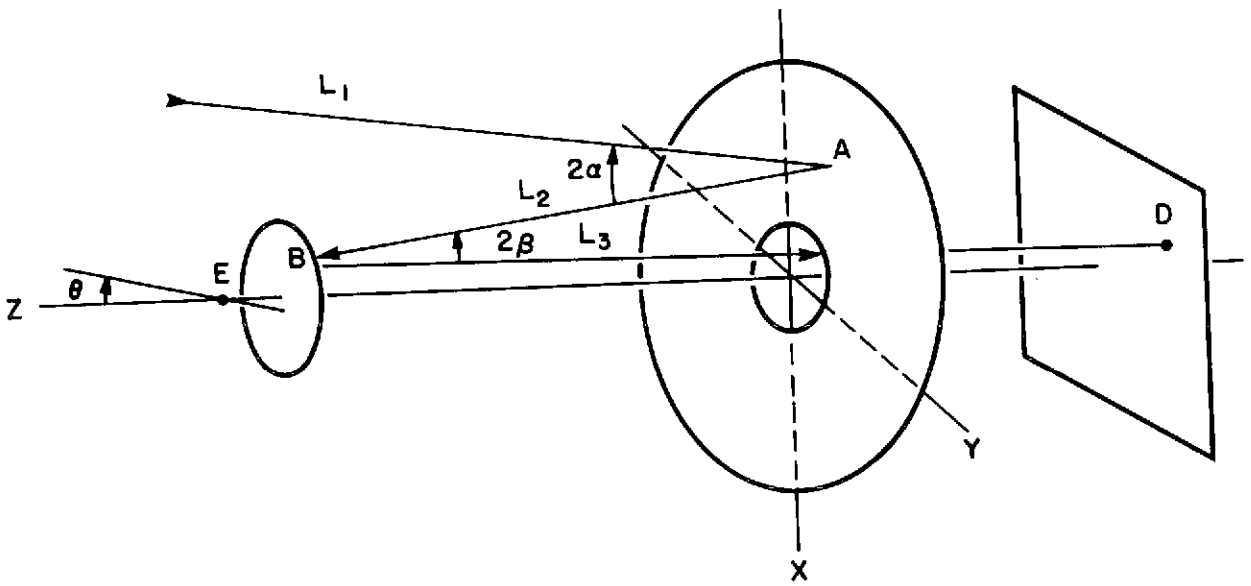

Figure 1.– Coordinates for the calculation. The origin is at the vertex of the primary mirror, whose axis is the z axis. The x axis is parallel to the axis of rotation of the secondary mirror.

pivots about point E through an angle θ which lies in the y-z plane. Parameters in the calculation are

c on-axis distance from center of primary surface to image plane

D_p diameter of primary mirror

D_s diameter of secondary mirror

e_p eccentricity of primary mirror

e_s eccentricity of secondary mirror

F_p $r_p/2$ focal length of primary paraxial sphere

r_p radius of curvature of primary mirror

r_s radius of curvature of secondary mirror

z_L on-axis distance from center of primary surface to image plane

z_s on-axis distance from center of primary surface to untilted secondary surface

γ object angle in the y-z plane

All these quantities except z_L are typically positive. Ray L_1 makes an angle α with the normal to the primary at point A and L_2 makes an angle β with the normal to the secondary at point B.

A few simple formulae are useful. The equivalent f number of the system is

$$f_e = \frac{z_s - z_L}{D_s} \tag{1}$$

The relationship between the radius of curvature of the secondary (r_s) and the focal length of the paraxial primary sphere (F_p) is

$$\frac{1}{F_p - z_s} - \frac{1}{z_s - z_L} = \frac{2}{r_s} \tag{2}$$

A typical application of equation (2) is to find the distance to the secondary given F_p, z_L, and r_s; the solution is

$$z_s = \frac{1}{2}\{F_p + z_L - r_s + [r_s^2 + (F_p - z_L)^2]^{1/2}\} \tag{3}$$

The variation in focal distance for a small change in secondary mirror position is given by

$$\delta \equiv \frac{dz_L}{dz_s} = 1 + \left(\frac{z_s - z_L}{F_p - z_s}\right)^2 \tag{4}$$

The underfilled primary diameter is

$$D_{pu} = \frac{F_p D_s}{F_p - z_s} \tag{5}$$

and the plate scale (angular displacement of the object in arc-min required for a 1-mm displacement of the image) is

$$S = \frac{3438'}{f_e \cdot D_{pu}} \tag{6}$$

The angle of tilt of the secondary (θ) determined by the beam angle in the sky (γ) and the on-axis detector is

$$\theta = \frac{r_s}{r_s - c} \frac{F_p}{F_p - z_s} \frac{\gamma}{2} \tag{7}$$

Equations (2) to (7) do not consider the figure of the mirrors, but are good approximations in practical cases.

Appendix A gives a brief analysis of Cassegrain-type telescopes similar to that of Jones (ref. 4) with a view to determining the mirror parameters for a particular configuration. Appendix B gives some approximate expressions useful in estimating effects that tend to overfill the primary. Appendix C describes the details of the ray-trace calculation.

The ray-trace program uses the parameters listed under Description of Calculation to compute the secondary tilt angle θ necessary to center the image, the unobscured primary area (underfilled primary area minus secondary mirror surface area), the f number of the secondary cone, the plate scale in the image plane, and the positions at the primary surface of the two extreme rays, which are rays reflected to the edges of the secondary mirror surface in the y-z plane. Then the program fills the unobscured aperture with a uniform distribution of parallel rays incident at the specified beam angle γ. Each ray is labeled with a symbol, of which the first 44 are distinct and the remainder are asterisks. The program lists the coordinates of the rays incident on the primary and then plots this pattern on the line printer. With this incident beam, the program calculates the centered image pattern and plots the pattern in the image plane. Alternatively, an arbitrary tilt-angle θ can be used, for which the program computes an off-axis image.

The angular resolution of the telescope is diffraction limited for wavelengths greater than some value λ_c, corresponding to the finite image size of a point object. The angular diameter (in arc-min) of the first dark ring of the diffraction pattern for wavelength λ is

$$\phi \approx \frac{2.44(3438)\lambda}{D_{pu}} \tag{8}$$

About 84 percent of the radiation falls within an angular diameter given by equation (8) for the diffraction pattern from a circular aperture of diameter D_{pu}. The program calculates a "diffraction diameter" d of a circular aperture that contains about 84 percent of the rays in the image plane. Setting $\phi \approx Sd$ for $\lambda = \lambda_c$ and using equation (6), one obtains

$$\lambda_c \approx \frac{d}{2.44\ f_e} \tag{9}$$

The program uses equation (9) to estimate λ_c.

EXAMPLES

The parameters for the three telescopes considered are given in table 1. All distances are given in millimeters. Values for the eccentricities were calculated from the formulae of appendix A. Values of z_s, f_e, δ, and θ/γ were determined from equations (3), (1), (4), and (7), respectively.

Figure 2 shows images calculated for the Lear telescope using the parameters from the first row of table 1. The input pattern covers the useful area of the primary (fig. 2(a)). The finite size of the centered image from an on-axis point object (fig. 2(b)) shows that the telescope is not figured precisely for this configuration. That the telescope is well focused is indicated by the thorough mixing of the rays from the input pattern. The diffraction diameter is 0.06 mm, and 85 percent of the rays lie within a circle of this diameter. For this configuration, the telescope is diffraction-limited for wavelengths greater than about 3.4μ. Figure 2(c) shows the image of a point object 5 arc-min off-axis when the secondary is untilted. The image appears nearly centered at the origin of the plot, which is displaced in this case from the axis of the telescope by 2.81 mm, corresponding to the 5 arc-min separation of the source from the telescope axis. Note that the scale size is twice that of figure 2(b). Figure 2(d) shows the on-axis image (centered by tilting the secondary mirror) of an object 5 arc-min off-axis. The scale is a factor of 2 larger than in figure 2(c). The aberrations incurred by centering the image of an off-axis object by tilting the secondary are coma-like and somewhat worse than those where the secondary is not tilted and the image is allowed to fall off-axis.

Figure 3 shows calculated images for the Lear telescope in a configuration determined by the parameters of the second example in table 1. The large back-focal distance (equal to the primary diameter) of this configuration is far from that for which the primary was figured. This accounts for the rather large on-axis image of an on-axis point source shown in figure 3(a). Figure 3(b) shows the on-axis image of a point source 12 arc-min off-axis. For this case, $d \approx 0.35$ mm, and the telescope is diffraction-limited for wavelengths greater than $\lambda_c \approx 23\mu$. The large beam throw in this example does not appreciably increase the image size over the on-axis case (fig. 3(a)) because - as noted above - the telescope is far from optimized at this large back-focal distance.

Theoretical images for the AIROscope telescope are shown in figure 4. Figure 4(a) shows the on-axis case and figure 4(b), the centered image of a point source 4 arc-min off-axis. The diffraction diameter of the latter image is 0.31 mm, corresponding to $\lambda_c = 11\mu$. In this example, the two images

TABLE 1.- PARAMETERS FOR SAMPLE CALCULATIONS SHOWN IN THE FIGURES.

Telescope[a]	D_p, mm	r_p, mm	e_p, —	D_s, mm	r_s, mm	e_s, —	c, mm	z_L, mm	z_S, mm	f_e, —	D_{pu}, mm	S, '/mm	δ, —	θ/γ, —	γ, '
Lear	305	919	0.82	78	325	0	20	-186	336.1	6.7	289	1.77	18.7	2.0	5.0
Lear	305	919	.82	99	435	0	20	-305	299.6	6.0	288	1.99	15.2	1.5	12.0
AIROscope	711	2840	.89	124	615	0	18	-284	1166	11.7	693	.42	33.6	2.9	4.0
C-141	914	3657	1.00	187	923	1.35	10	-1219	1435	14.2	868	.28	47.1	2.4	3.0
C-141	914	3657	1.00	187	899	1.28	10	-1752	1435	17.0	868	.23	65.4	2.4	3.0

[a]Used in infrared astronomy at Ames.

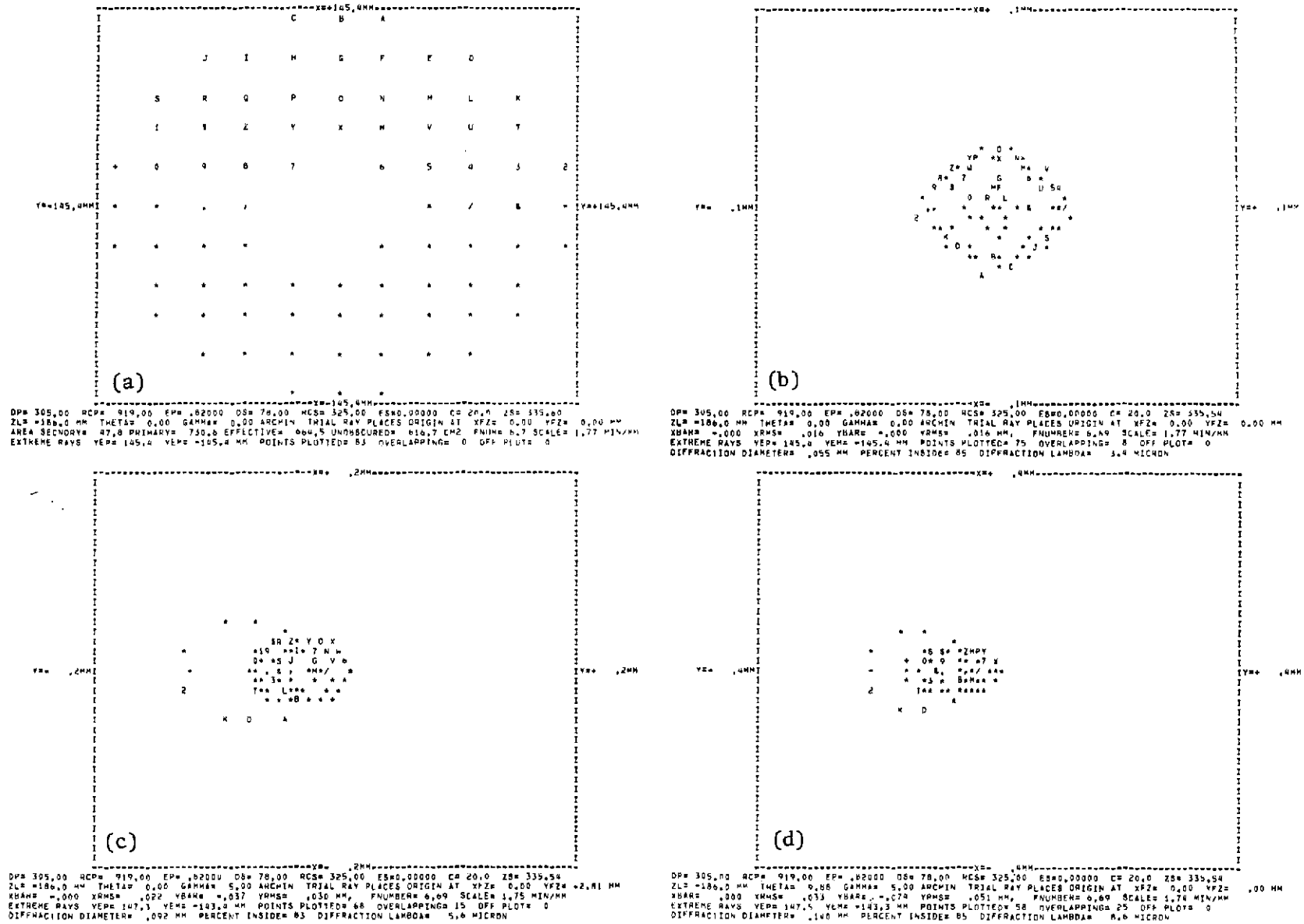

Figure 2.— Calculations for the Lear jet telescope using the parameters from the first example in table 1. (a) Input pattern. (b) Image of an on-axis point object with secondary untilted. (c) Image of a point object 5 arc-min off-axis with secondary untilted. (d) Same as (c) but with secondary tilted to center the image on axis.

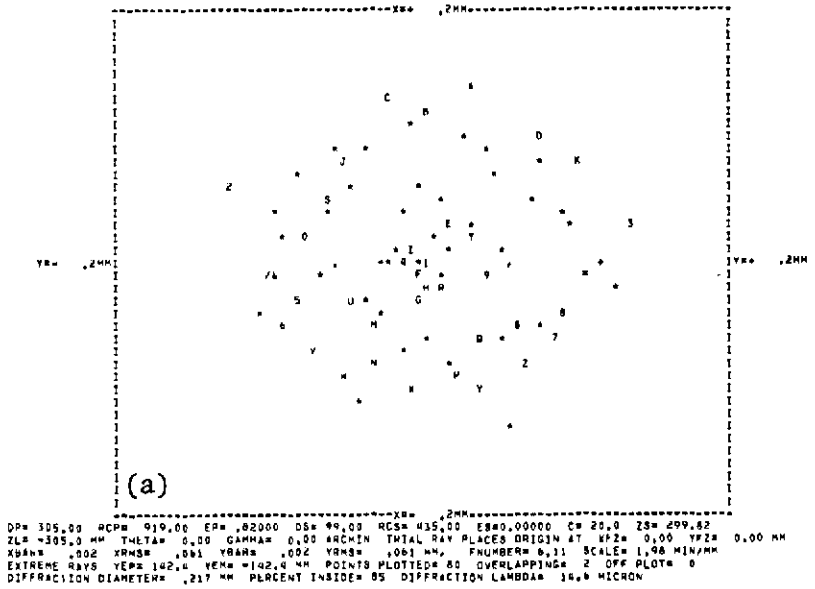

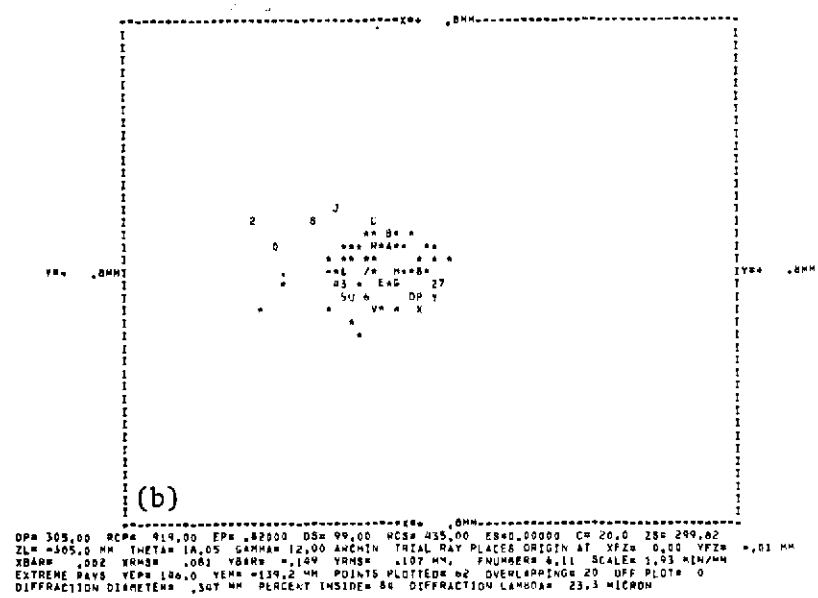

Figure 3.— Calculations for the Lear jet telescope using the parameters from the second line in table 1. (a) Focused on-axis image of an on-axis point source. (b) On-axis image of a point source 12 arc-min off-axis.

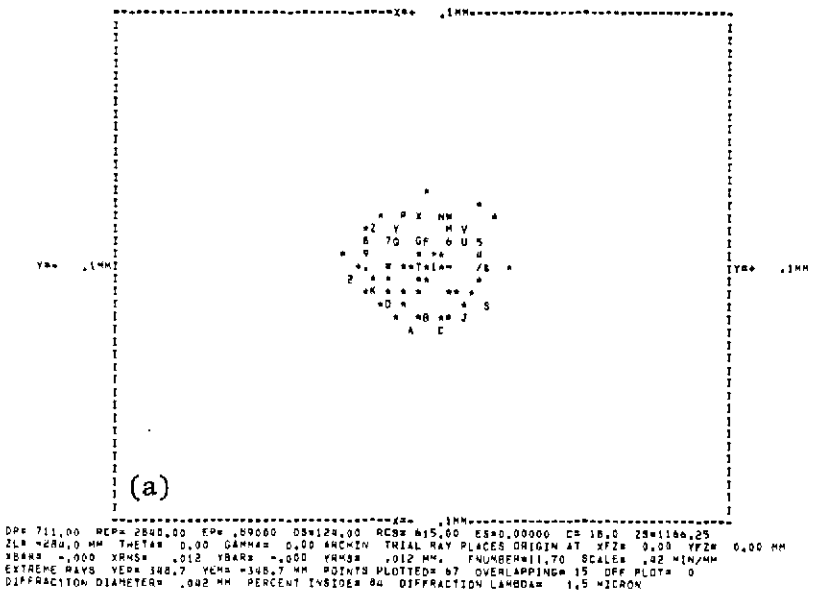

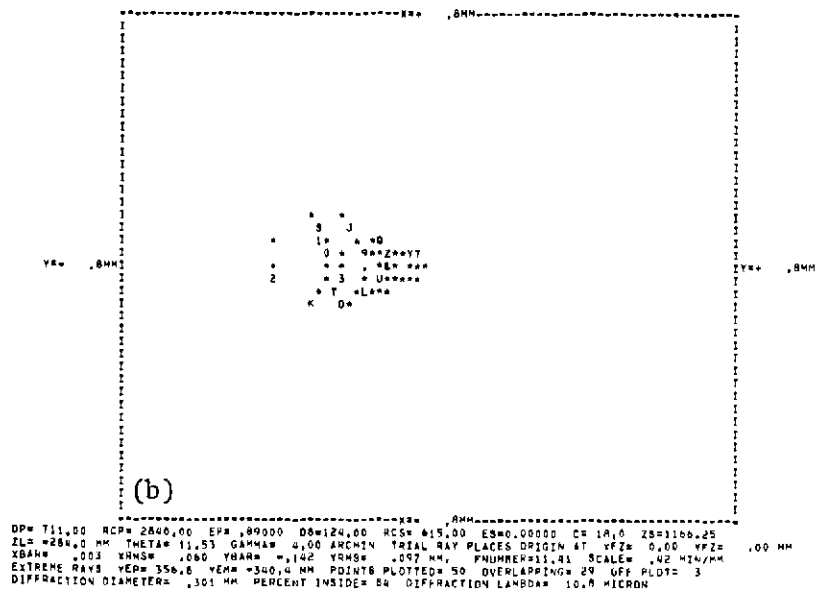

Figure 4.— Images for the AIROscope telescope. (a) Focused on-axis image of an on-axis point source. (b) On-axis image of a point source 4 arc-min off-axis.

differ considerably in size because of the aberrations of the tilted secondary, off-axis object configuration considered in figure 4(b).

Figure 5(a) shows images for the C-141 telescope in the design configuration, except that the secondary mirror diameter has been reduced to underfill the primary. Note that the design configuration results in good image quality for on-axis objects, as expected. The centered image for a point source 3 min off-axis is shown in figure 5(b). The diffraction diameter is 0.16 mm, which corresponds to $\lambda_c = 4.6\mu$.

Figure 6 shows images for the last example in table 1. This back-focal distance is longer than the previous example and corresponds to an instrument somewhat behind the intended image plane. The secondary in the calculation has been refigured for this application, but the primary is as shown in figure 5. The quality of the image is comparable to that of the design configuration (compare figs. 6(a) and 6(b) with figs. 5(a) and 5(b)). Although the diffraction diameter is larger for figure 6(b) than for figure 5(b), the diffraction-limiting wavelength λ_c is about the same because of the difference in f_e for these two systems.

CONCLUDING REMARKS

The quality of the image calculated by the program described here is somewhat better than the systems represented because of imperfections in the optics. Image quality similar to that calculated here has been observed with the Lear jet telescope and the C-141 telescope.

The advantage of the ray tracing analysis over an approximate analytical treatment is that ray tracing includes the effects of all aberrations simultaneously and yields a quantitative distribution of the energy in the image. This permits a simple comparison with the diffraction distribution and provides experimenters with a convenient summary of the anticipated optimum telescope performance for a given configuration.

The most serious type of aberration encountered - third-order coma - can be reduced using the optics design of Bottema and Woodruff (ref. 3) and should probably be done when one designs a telescope for use with an OSM.

Ames Research Center
National Aeronautics and Space Administration
Moffett Field, Calif., October 18, 1974

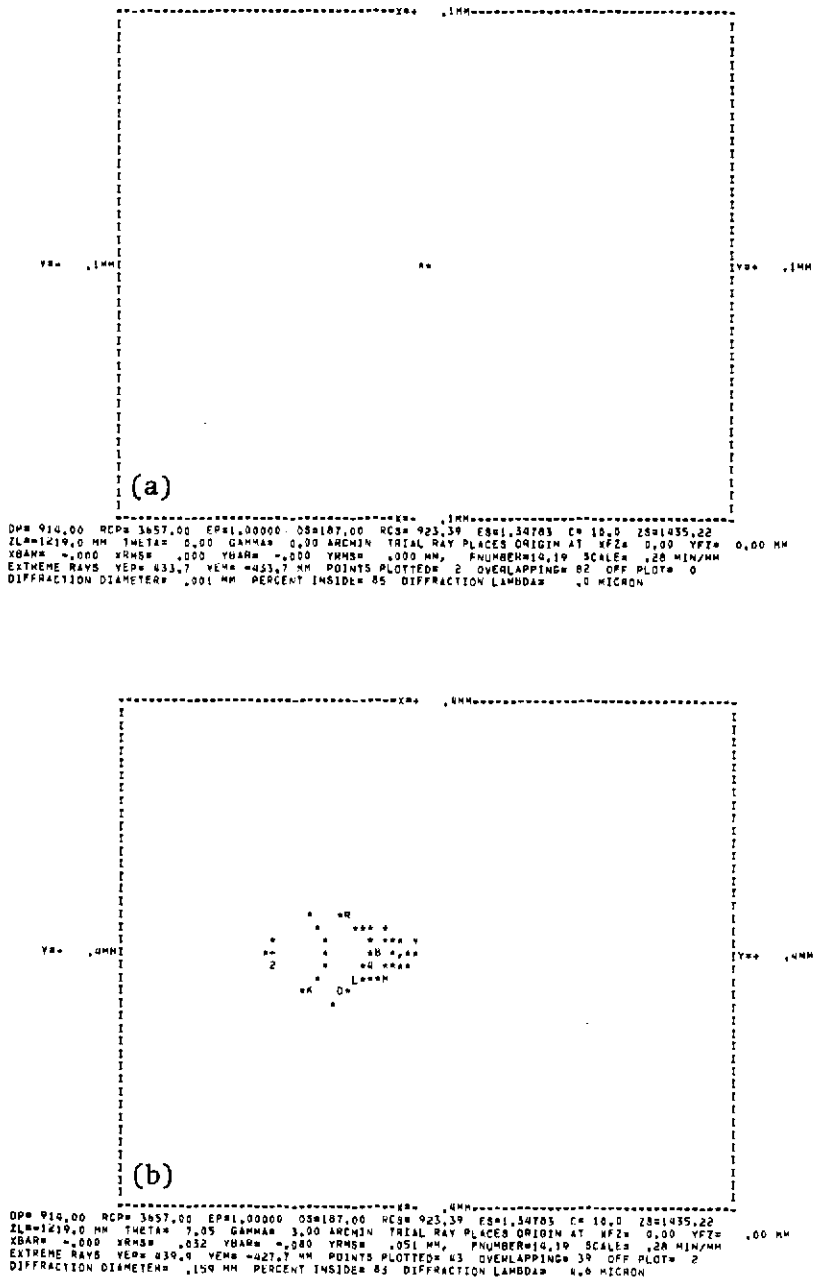

Figure 5.— Images for the C-141 telescope at the nominal bent-Cassegrain focal plane. (a) Focused on-axis image of an on-axis point source. (b) On-axis image of a point source 3 arc-min off-axis.

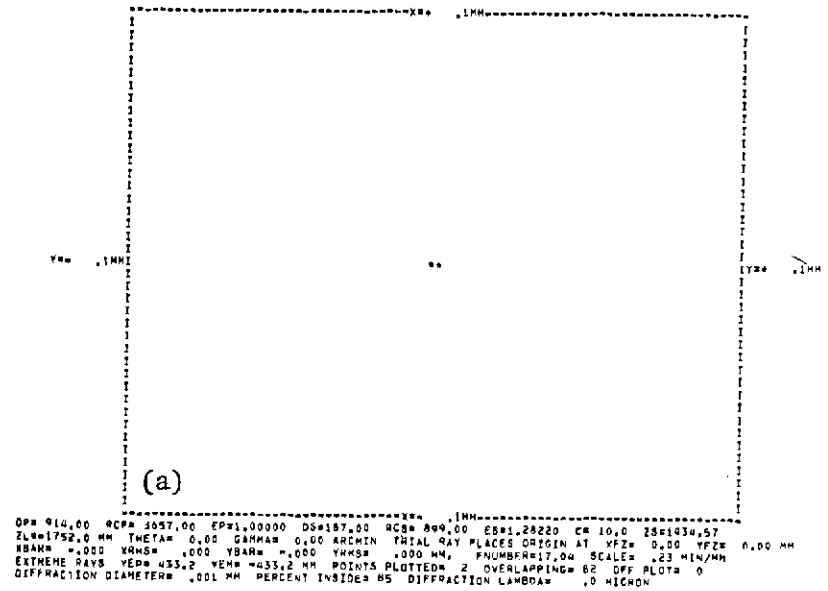

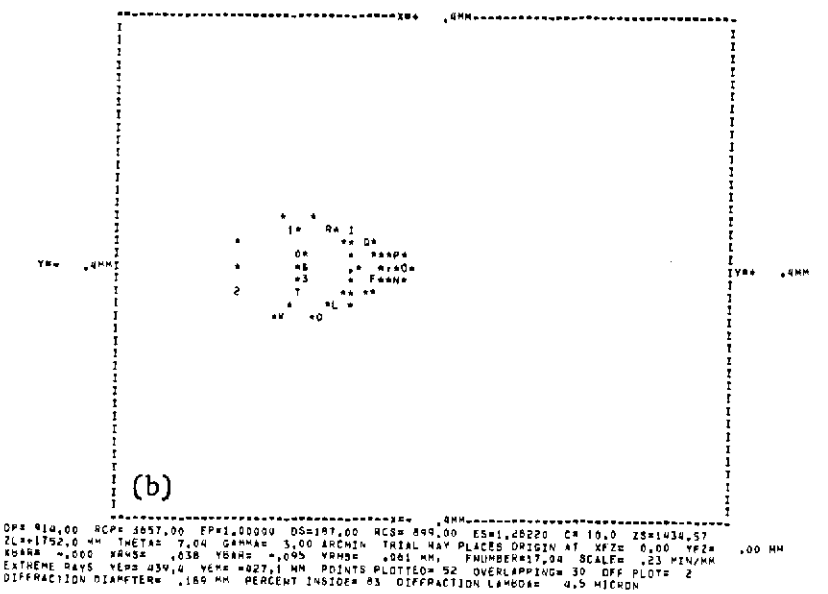

Figure 6.— Images for the C-141 telescope at the "backplate" bent-Cassegrain focal plane for the parameters of the last example in table 1. (a) Focused on-axis image of an on-axis point source. (b) On-axis image of a point source 3 arc-min off-axis.

APPENDIX A

ANALYTICAL ANALYSIS OF CASSEGRAIN-TYPE TELESCOPES

For a ray-trace analysis one must have the radii, eccentricities, and diameters of the mirror surfaces as well as the mirror separations. The eccentricities are often not readily available and are not easily measured. This appendix outlines the formalism used to describe the mirror surfaces for the ray trace calculation and to show how the eccentricities are calculated. The approach follows the development of Jones (ref. 4) and can be applied to any Cassegrain-type telescope with reflectors made of conic sections. The classical Cassegrain and Dall-Kirkham geometries are treated explicitly.

A conic section with a vertex at the origin and symmetric for $x > 0$[1] is given by

$$y^2 - 2rx + (1 - e^2)x^2 = 0 \tag{A1}$$

where $e \geq 0$ is eccentricity, $r = ed$, and d is the distance from the focus to the directrix. The distance from the vertex to the nearest focus of the conic is

$$x_F = \frac{r}{1 + e} \tag{A2}$$

The four standard cases are

Figure	Usual formula	e	r
Circle	$x^2 + y^2 = r^2$	0	r
Ellipse	$x^2/a^2 + y^2/b^2 = 1$	$\sqrt{1 - b^2/a^2} < 1$	b^2/a
Parabola	$y^2 - 4ax = 0$	1	2a
Hyperbola	$x^2/a^2 - y^2/b^2 = 1$	$\sqrt{1 + b^2/a^2} > 1$	b^2/a

For the ellipse and hyperbola, the distance between foci is

$$2ae = \frac{2re}{|1 - e^2|} \tag{A3}$$

From equation (A1), x is an even function of y; with $p \equiv 1 - e^2$, one finds that

[1]All calculation in this appendix is done in a two-dimensional coordinate system with axes labeled x and y.

$$x = \frac{r}{p}\left[1 - \left(1 - \frac{py^2}{r^2}\right)^{1/2}\right] = \frac{y^2}{2r} + \frac{p}{8r^3}\,y^4 + \frac{p^2}{16r^5}\,y^6 + \ldots \qquad \text{(A4)}$$

Consideration of equation (A1) for $e = 0$ clearly shows that r is the radius of the sphere that fits all the conic surfaces near the vertex - the so-called paraxial sphere. A conic section with its vertex at the origin may thus be characterized by parameters r, e, and maximum diameter D.

In a classical Cassegrain, the primary surface is a paraboloid and the secondary is a hyperboloid. The secondary is chosen so that one of its foci coincides with the prime focus and the other is the Cassegrain focus. In this geometry, an incident beam of light parallel to the axis focuses to a point at the Cassegrain focus. The determination of the mirror parameters is straightforward: the effective primary diameter D_p and focal length F_p are usually ordained by practical considerations. Of course, $e_p = 1$ and $r_p = 2F_p$. The distance L from the prime focus to the Cassegrain focus is given by equation (A3):

$$L = \frac{2r_s e_s}{|1 - e_s^2|} \qquad \text{(A5)}$$

The plate scale of the telescope is the ratio of the object angular size to the image physical size and is determined by the equivalent focal length F_p'; this is the focal length of a parabola of diameter D_p which has the same cone angle as the secondary:

$$F_p' = D_p\left(\frac{F_s}{D_s}\right) \equiv AF_p \qquad \text{(A6)}$$

Here F_s is the distance from the secondary to the Cassegrain focus, D_s is the *effective* diameter of the secondary, and A is the amplification. Sketch (a) shows the various dimensions. (In the notation used in the text, $L = F_p - z_L$ and $F_s = z_s - z_L$.)

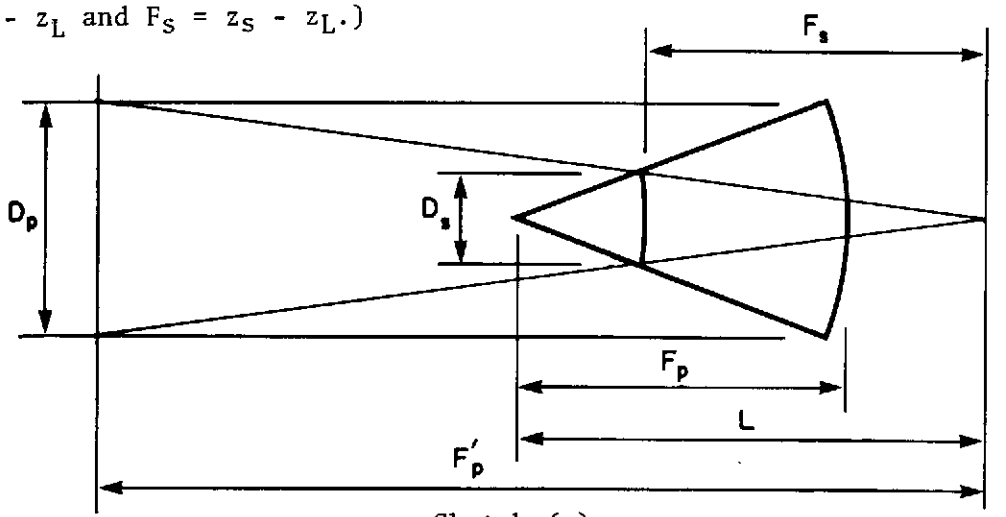

Sketch (a)

The quantity D_s satisfies the geometrical relation

$$\frac{F_p}{D_p} \doteq \frac{L - F_s}{D_s} \tag{A7}$$

From equations (A6) and (A7), $L - F_s = L/(A + 1)$ so that

$$D_s = \frac{L}{(A + 1)(F_p/D_p)} \tag{A8}$$

Note that F_p/D_p is the f number of the primary and D_s need not be the physical diameter of the secondary. (If the secondary is undersized to avoid filling the primary, then D_s is the physical diameter of the secondary and D_p is the effective primary diameter.) Of course, equation (A8) is independent of the eccentricities of the surfaces. From equation (A2) and sketch (a),

$$L - F_s = \frac{r_s}{1 + e_s} \tag{A9}$$

The combination of equations (A5) through (A7) and (A9) yields

$$r_s = \frac{2LA}{A^2 - 1} \tag{A10a}$$

$$e_s = \frac{A + 1}{A - 1} \tag{A10b}$$

for the parameters of the secondary in a true Cassegrain system. The result for r_s is the same if one uses the spherical mirror formula, equation (2), which demonstrates the advantage of this approach, namely, that the fundamental mirror parameters are the eccentricities of the conics and the radii of the corresponding paraxial spheres.

Consider now the modification of the Cassegrain geometry to include other (conic) surfaces. Since equations (A8) and (A10a) still hold, one needs to determine only e_p and e_s. According to equation (A4), one can write for the primary surface

$$x_p \simeq \frac{y_p^2}{2r_p} + P\frac{y_p^4}{(2r_p)^3} \tag{A11a}$$

and, for the secondary surface,

$$x_s \simeq \frac{y_s^2}{2r_s} + \left[S - \frac{4A}{(A - 1)^2}\right]\frac{y_s^4}{(2r_s)^3} \tag{A11b}$$

Here P and S are parameters that describe the deformed surfaces (P = S = 0 for the true Cassegrain geometry) and equation (A10b) has been used to eliminate the eccentricity of the hyperboloidal secondary. The coordinates of each surface are measured from its intersection with the x axis. Deviations from the standard surfaces are

$$\Delta x_p \simeq P\left[\frac{y_p^4}{(2r_p)^3}\right] \tag{A12a}$$

$$\Delta x_s \simeq S\left[\frac{y_s^4}{(2r_s)^3}\right] \tag{A12b}$$

for the primary and secondary, respectively. Spherical aberration can be corrected if the deformations of the primary and secondary surfaces are equal for corresponding zones, that is,

$$\Delta x_p(y_p) = \Delta x_s(y_s) \tag{A13a}$$

with

$$\frac{y_p}{y_s} = \frac{D_p}{D_s} \tag{A13b}$$

From equations (A12) and (A13), the condition for zero spherical aberration is

$$P \simeq S\left(\frac{r_p}{r_s}\right)^3\left(\frac{D_s}{D_p}\right)^4 \tag{A14}$$

Equation (A14) thus relates the deformation parameters for the surfaces of a modified Cassegrain telescope corrected for spherical aberration.

For example, the Dall-Kirkham geometry uses a spherical secondary to facilitate construction and modification of the telescope. Comparing equations (A4) and (A11b), one finds that

$$S = 1 + \frac{4A}{(A - 1)^2} \tag{A15}$$

since $e_s = 0$. From equations (A14) and (A15) and the fact that $P = 1 - e_p^2$, it follows that

$$e_p = \left[1 - \left(\frac{A + 1}{A - 1}\right)^2\left(\frac{r_p}{r_s}\right)^3\left(\frac{D_s}{D_p}\right)^4\right]^{1/2} < 1 \tag{A16}$$

so that the primary surface is ellipsoidal. If expression (A10a) is substituted for r_s and (A8) for D_s into (A16), one obtains, for the Dall-Kirkham geometry, a primary eccentricity of

$$e_p = \left(1 - \frac{A^2 - 1}{A^3}\frac{L}{F_p}\right)^{1/2} \tag{A17}$$

APPENDIX B

CALCULATION OF RESTRICTIONS ON USEFUL APERTURE

Equation (5), $D_{pu} = F_p D_s/(F_p - z_s)$, gives the underfilled primary diameter D_{pu} for an on-axis point source if one assumes that the secondary mirror is intentionally undersized. Here approximate expressions are given for increments to $(1/2)D_{pu}$ due to other common effects. These expressions are useful in determining the secondary mirror diameter (D_s) when one designs the secondary and in determining the amount of the primary used for a given application once the telescope has been configured. The notation used here is the same as that in the text.

A detector with a finite aperture extending a distance x_d from the telescope axis in the image plane will detect light reflected from a point on the primary a distance $(1/2)D_{pu} + \Delta x_1$ from the axis where

$$\Delta x_1 \simeq \frac{x_d z_s}{z_s - z_L} \tag{B1}$$

If the detector aperture is chosen to diffraction-limit the telescope at wavelengths greater than λ_d, then equation (9) applies with $\lambda_d = \lambda_c$ and $x_d = (1/2)d$. From equations (9) and (1), equation (B1) becomes

$$\Delta x_1 \simeq \frac{1.22\lambda_d z_s}{D_s} \tag{B2}$$

To mount different instruments on the telescope, some adjustment of the focus must be provided. The primary aperture will increase as the image plane is moved closer to the primary for a secondary of fixed diameter. If Δz_L is the distance the image plane is moved from the nominal position, the increase in the radius of the primary aperture is

$$\Delta x_2 \simeq \frac{D_{pu}\Delta z_L}{(F_p - z_s)\delta} \tag{B3}$$

where δ is given by equation (4).

Equations (B1) to (B3) assume that the secondary is untilted. These effects are not included in the ray trace calculation. When the secondary is tilted to center the image of an object which is off-axis by an angle γ, the extent of the primary used in the plane of the tilt is $\Delta x_3 + (1/2)D_{pu}$, where

$$\Delta x_3 \leq \frac{z_s F_p}{F_p - z_s}\gamma \tag{B4}$$

This effect is calculated more accurately by the ray trace program. The value obtained from equation (B4) is an overestimate.

As an example, consider the Δx terms corresponding to the first case in table 1. If a 5-mm-diameter detector aperture on axis (corresponding to an 8.85 arc-min full-width FOV) is assumed, then $x_d = 2.5$ mm and

$$\Delta x_1 \simeq 1.6 \text{ mm} \tag{B5a}$$

If $\lambda_d = 150\mu$, then

$$\Delta x_1' \simeq 0.8 \text{ mm} \tag{B5b}$$

Note that this corresponds to a diffraction diameter $d = 2.5$ mm. If the image plane is moved closer to the primary by $\Delta z_L = 25$ mm, equation (B3) gives

$$\Delta x_2 \simeq 7.5 \text{ mm} \tag{B5c}$$

For a beam throw of $\gamma = 5$ arc-min,

$$\Delta x_3 \lesssim 3.3 \text{ mm} \tag{B5d}$$

The true value of Δx_3 obtained from the ray trace program (figs. 2(b) and 2(c)) is 1.9 mm. Since, for this example, $D_{pu} = 289$ mm and $D_p = 305$ mm, Δx_1, $\Delta x_1'$, and Δx_3 are not sufficient to fill the primary. On the other hand, the value of Δx_2 would cause the primary to be filled and presumably be unacceptable for work beyond about 3μ, due to the power reaching the detector from the telescope support structure.

APPENDIX C

DETAILS OF RAY TRACE CALCULATION

Rays L_1, L_2, and L_3 have direction cosines c_{1j}, c_{2j}, and c_{3j}, respectively, with $j = x$, y, and z. From appendix A, the equation of the primary is written

$$\Phi_p = x^2 + y^2 + (1 - e_p^2)z^2 - 2r_p z = 0 \tag{C1}$$

Since secondary pivots through angle θ about an axis parallel to the x axis through the pivot point at E, the equation of the secondary is

$$\left.\begin{aligned} &\Phi_s = x^2 + y'^2 + (1 - e_s^2)z'^2 - 2r_s z' = 0 \\ &\text{where} \\ &y' = (z - z_o)\sin\theta + (y - y_o)\cos\theta \ , \\ &z' = (z - z_o)\cos\theta - (y - y_o)\sin\theta \ , \\ &\text{and} \\ &y_o = c \sin\theta \\ &z_o = z_s + c(1 - \cos\theta) \end{aligned}\right\} \tag{C2}$$

Here c is the distance from E to the center of the secondary surface, which is located at y_o, z_o. Equation (C2) can conveniently be rewritten in the form

$$\left.\begin{aligned} &\Phi_s = x^2 + a_1(y - y_o)^2 + a_2(z - z_o)^2 + 2a_3(y - y_o)(z - z_o) \\ &\qquad +2a_4(z - z_o) + 2a_5(y - y_o) = 0 \\ &\text{where} \\ &a_1 = 1 - e_s^2 \sin^2\theta \\ &a_2 = 1 - e_s^2 \cos^2\theta \\ &a_3 = \frac{1}{2} e_s^2 \sin 2\theta \\ &a_4 = -r_s \cos\theta \\ &a_5 = r_s \sin\theta \end{aligned}\right\} \tag{C3}$$

The unit outward normal to one of these surfaces is

$$\hat{n}_i = \frac{\nabla\Phi_i}{|\nabla\Phi_i|} \tag{C4}$$

where $i = p$ or s. Given $\hat{L}_1$, one has

$$\left.\begin{aligned} \hat{L}_1 \cdot \hat{n}_p &= -\hat{L}_2' \cdot \hat{n}_p \equiv \cos\alpha > 0 \\ |\hat{L}_1 \times \hat{n}_p| &= |\hat{L}_2 \times \hat{n}_p| = \sin\alpha \geq 0 \end{aligned}\right\} \tag{C5}$$

The equation of $\hat{L}_2$ is then obtained from equation (B5):

$$\hat{L}_2 = \hat{L}_1 - 2\hat{n}_p \cos\alpha \tag{C6}$$

If

$$\vec{m}_2 = \frac{\hat{L}_2}{L_{2z}} \tag{C7}$$

then points lying on $\hat{L}_2$ satisfy

$$\left.\begin{aligned} x - x_A &= m_{2x}(z - z_A) \\ y - y_A &= m_{2y}(z - z_A) \end{aligned}\right\} \tag{C8}$$

where A denotes the intersection of $\hat{L}_1$ with the primary.

The simultaneous solution of equations (C3) and (C8) gives the intersection of $\hat{L}_2$ with the secondary at point B. One finds a quadratic equation for $u = z_B - z_A$, with the result

$$u = -\frac{B + (B^2 - AC)^{1/2}}{A} \tag{C9}$$

where

$$\left.\begin{aligned} A &= m_{2x}^2 + a_1 m_{2y}^2 + a_2 + 2a_3 m_{2y} \\ B &= m_{2x}x_A + a_1 m_{2y} w_y + a_2 w_z + a_3(w_y + m_{2y} w_z) + a_4 + a_5 m_{2y} \\ C &= x_A{}^2 + a_1 w_y{}^2 + a_2 w_z{}^2 + 2a_3 w_y w_z + 2a_4 w_z + 2a_5 w_y \\ w_j &= j_A - j_o \,, \qquad j = x, y, z \end{aligned}\right\} \tag{C10}$$

The coordinates of point B are then

$$\left.\begin{aligned} x_B &= x_A + m_{2x}u \\ y_B &= y_A + m_{2y}u \\ z_B &= z_A + u \end{aligned}\right\} \tag{C11}$$

The same procedure which led to equation (C6) gives

$$\hat{L}_3 = \hat{L}_2 + 2\hat{n}_S \cos \beta \tag{C12}$$

where equations (C3), (C4), and (C11) are used to obtain $\hat{n}_S$ and $\cos \beta = -\hat{L}_2 \cdot \hat{n}_S$. As in equation (C7), one defines

$$\vec{m}_3 = \frac{\hat{L}_3}{L_{3z}} \tag{C13}$$

If the image plane is at $z = z_L$, then the intersection with $\hat{L}_3$ is given by

$$\left.\begin{aligned} x_D &= x_B + (z_L - z_B)m_{3x} \\ y_D &= y_B + (z_L - z_B)m_{3y} \end{aligned}\right\} \tag{C14}$$

which is the desired result.

REFERENCES

1. Aumann, H. H.; Gillespie, C. M., Jr.; and Low, F. J.: The Internal Powers and Effective Temperatures of Jupiter and Saturn. Ap. J. Letters, vol. 157, 1969, p. L69.

2. Dicke, R. H.: The Measurement of Thermal Radiation of Microwave Frequencies. Rev. Sci. Instr., vol. 17, 1947, p. 268.

3. Bottema, M.; and Woodruff, R. A.: Third-Order Aberrations in Cassegrain-Type Telescopes and Coma Corrections in Servo-Stabilized Images. Applied Optics, vol. 10, 1971, p. 300.

4. Jones, R. T.: Coma of Modified Gregorian and Cassegrainian Mirror Systems. J. Opt. Soc. Amer., vol. 44, 1954, p. 630.

NASA-Langley, 1975 A-5657